NUCL SCI TECH (2019) 30:141
https://doi.org/10.1007/s41365-019-0663-6

Stellar reaction rate of ^{55}Ni(p, γ)^{56}Cu in Type I X-ray bursts

Shao-Bo Ma[1,2] · **Li-Yong Zhang**[3] · **Jun Hu**[1,2]

Received: 15 May 2019 / Revised: 3 June 2019 / Accepted: 10 June 2019 / Published online: 13 August 2019

Abstract ^{56}Cu is close to the waiting-point nucleus ^{56}Ni and lies on the rapid proton capture (rp) process path in Type I X-ray bursts (XRBs). In this work, we obtained a revised thermonuclear reaction rate of ^{55}Ni(p, γ)^{56}Cu in the temperature region relevant to XRBs. This rate was recalculated based on the recent experimental level structure in ^{56}Cu, the recently measured proton separation energy of S_p = 579.8(7.1) keV, together with shell-model calculation, and the mirror nuclear structure in ^{56}Co. The associated uncertainties in the rates were estimated by a Monte Carlo method. Our revised rate is significantly different from the recent results, which were partially based on experimental results; in addition, we found that a result in a previous work was incorrect. We recommend our revised rate to be incorporated in the future astrophysical network calculations.

This work was supported by the National Natural Science Foundation of China (Nos. 11825504, 11490562, and 11675229), and the Major State Basic Research Development Program of China (No. 2016YFA0400503).

✉ Li-Yong Zhang
liyongzhang@bnu.edu.cn

Jun Hu
hujunbaggio@impcas.ac.cn

[1] Institute of Modern Physics, Chinese Academy of Sciences, Lanzhou 730000, China

[2] University of Chinese Academy of Sciences, Beijing 100049, China

[3] College of Nuclear Science and Technology, Beijing Normal University, Beijing 100875, China

Keywords Nuclear astrophysics · Reaction rate · X-ray burst

1 Introduction

Type I X-ray bursts (XRBs) are triggered by thermonuclear runaways in the accreted envelopes of neutron stars in close binary systems [1, 2]. During the thermonuclear runaway, the accreted envelope enriched in H and He can be transformed to matter strongly enriched in heavier species (up to $A \simeq 100$ [3, 4]) via the rapid proton capture process (rp-process) [5–7]. The physical theory of the XRBs has been reviewed in Refs. [8–10].

The rp-process is mostly characterized by localized (p,γ)–(γ,p) equilibrium within particular isotonic chains near the proton drip line. The abundance distribution within an isotonic chain exponentially depends on the difference in nuclear masses because the abundance ratio between two neighboring isotones is proportional to $\exp[S_p/kT]$, where S_p is the proton separation energy. In particular, isotonic chains with sufficiently small S_p values (relative to XRB temperatures at 1 GK and $kT \approx 100$ keV) need to be known with a precision of at least $\sim$50–100 keV [6, 11]. To compare model predictions with observations of the light curves [12], reliable nuclear physical inputs, such as the precise S_p values and thermonuclear reaction rates, are needed for those nuclei along the rp-process path.

^{56}Cu is a very important nucleus, because it is close to the waiting-point nucleus ^{56}Ni and lies on the rp-process path [6, 12]. In this work, a new thermonuclear reaction rate is derived for ^{55}Ni(p, γ)^{56}Cu in the temperature region relevant to XRBs based on the recent experimental results

of energy levels and proton separation energy of $S_p = 579.8(7.1)$ keV in ^{56}Cu, together with the shell-model calculation and mirror nuclear structure in ^{56}Co.

2 Proton separation energy of $S_p(^{56}Cu)$

Previously, four theoretical proton separation energy, S_p, values have been predicted for ^{56}Cu, as $S_p(^{56}Cu) = 573 \pm 54$ keV based on the charge-symmetry formula of Kelson–Garvey [13], 560 ± 140 keV from Coulomb displacement energy (CDE) mass relation [14], 526 ± 1 keV using the improved Kelson–Garvey (ImKG) mass relation [15], and 647 ± 88 keV based on the mirror symmetry and known data from beta-delayed proton spectroscopy [16]. Using the smoothness trends of the mass surface, analysis by atomic mass evaluations (AME) provided $S_p(^{56}Cu)$ values as 459 ± 200 keV in AME85 [17], 560 ± 140 keV in both AME95 [18] and AME03 [19], and 190 ± 200 keV in AME12 [20]. The large uncertainty in the results is due to the theoretically estimated mass of ^{65}Cu.

The first measurement of the nuclear mass of ^{65}Cu was first performed in 2016, with a relative precision of $(1-4) \times 10^{-7}$ using isochronous mass spectrometry (IMS) at the Cooler Storage Ring (CSRe), at the Institute of Modern Physics IMP in Lanzhou, China. Together with the unpublished mass excess value of $ME(^{65}Cu) = -38643(15)$ keV, the value of $S_p(^{56}Cu) = 596 \pm 15$ keV was compiled into AME16 [21] (referenced as "private communication"). This experimental value was formally published in 2018 [22]; however, during the review process of this paper, a more accurate value of $ME(^{65}Cu) = -38626.7(7.1)$ keV was measured [23] using the Low-Energy Beam and Ion Trap (LEBIT) 9.4-T penning trap mass spectrometer in the National Superconducting Cyclotron Laboratory (NSCL) at the Michigan State University (MSU). Then, an accurate value of $S_p = 579.8(7.1)$ keV was deduced. Based on the weighted average S_p values obtained from the MSU and IMP measurements, the value of $S_p = 582.8(6.4)$ keV was adopted in their thermonuclear $^{55}Ni(p,\gamma)^{56}Cu$ rate calculations [23]. This shows that two experimental ME values agree well within the uncertainties, and the S_p values also agree well with the three theoretical predictions mentioned above, except for the highly accurate ImKG prediction with an uncertainty of ± 1 keV [15].

In this work, in the reaction rate calculations we use the value of $S_p = 579.8(7.1)$ keV derived at MSU, because the MSU mass value of ^{65}Cu has been the most accurate value until now.

3 Previous results for reaction rates

The reaction rate of $^{55}Ni(p,\gamma)^{56}Cu$ was estimated for the first time by van Wormer et al. [24], based on the properties of 10 resonances in the mirror nucleus ^{56}Co, at $S_p = 459$ keV determined by AME85. This rate is referred to as *laur* in the JINA Reaclib Database [25]. Later, Fisker et al. [26] performed a shell-model calculation at the value of $S_p = 563$ keV estimated by AME95. The following comments need to be added about the study by Fisker et al. [26]: (1) the direct-capture (DC) rate, expressed by Eq. (15) in the paper, need to be multiplied by a factor of two; (2) considering the $^{55}Ni(p,\gamma)^{56}Cu$ reaction, certain resonance strength values listed in Table I in the paper (p. 270) cannot be reproduced by the relationship of $\omega\gamma = \omega\Gamma_p\Gamma_\gamma/(\Gamma_p + \Gamma_\gamma)$, based on their Γ_p and Γ_γ values; and (3) the resonant rate cannot be reproduced by the analytical formula in Eq. (7) in the paper using the listed strengths. Unfortunately, we cannot find the exact source of these errors. In addition, shell-model levels predicted by Fisker et al. for ^{56}Cu (with excitation energy up to $E_x = 3561$ keV) were only valid for a temperature region up to ~ 3.5 GK by considering the Gamow window. Therefore, the rates listed in Table II in Ref. [26] are typically underestimated above ~ 3.5 GK. In the JINA Reaclib Database, the rate calculated by Fisker et al. [26] was revised at the value of $S_p = 648$ keV, and denoted as *nfis*.

In addition, certain theoretical rates based on the statistical model are available in the JINA Reaclib Database [25]. For instance, the *rath, thra* rates are obtained from statistical model calculations [27] using the finite-range droplet macroscopic (FRDM) [28]($S_p = -448$ keV) and the ETSFIQ mass models [29] ($S_p = 1919$ keV), respectively. The *ths8* rate is the theoretical value by Rauscher [25] ($S_p = 648$ keV). These indicated that the rates from statistical models differ from one another by up to several orders of magnitude in the typical XRB temperature range. Therefore, experimental data for ^{56}Cu, such as the S_p value and level structure information, are strongly required.

In 2017, the low-lying energy levels of ^{56}Cu ($E_x = 166, 572, 826, 1037,$ and 1224 keV) were obtained by in-beam γ-ray spectroscopy using the state-of-art Gamma-Ray Energy Tracking In-beam Nuclear Array (GRETINA) detector together with the S800 spectrograph at MSU [30]. With the newly obtained value of

$S_p = 639 \pm 82$ keV using a more localized isobaric multiplet mass equation (IMME) fit, the ^{55}Ni$(p,\gamma)^{56}$Cu rate was calculated together with the shell-model results. In this study, this rate is denoted as *ong*.

As mentioned in the previous section, the high-precision mass measurement of ^{56}Cu was performed at MSU in 2018 [23]: Valverde et al. obtained a weighted average value of $S_p = 582.8(6.4)$ keV and applied it in the reaction rate calculations. In that study, the energy levels observed in Ref. [30] were utilized, and the resonance energies and corresponding proton width, Γ_p, were scaled to the revised S_p value. Although the reaction rates and the associated uncertainties were calculated and presented in a figure, no numerical rates were provided for the readers. In this study, this rate is denoted as *valverde*.

4 Energy levels in ^{56}Cu

As mentioned in the previous section, Ong et al. [30] observed five low-lying energy levels, $E_X = 166, 572, 826, 1037$, and 1224 keV, in ^{56}Cu, using in-beam γ-ray spectroscopy at MSU [30]. Orrigo et al. [31] performed a β-delayed-proton decay experiment of ^{56}Zn at the Grand Accélérateur National d'Ions Lourds (GANIL), and observed six proton-decay branches. Based on these events, the level scheme of ^{56}Cu was constructed in the range of $E_X = 1391$–3508 keV. The associated large uncertainty of 140 keV was due to the uncertainty of $S_p = 560 \pm 140$ keV estimated by AME03 at that time. In this work, the excitation energies obtained by Orrigo et al. are shifted by 19.8 keV (i.e. to 579.8–560.0 keV) upward, to $E_X = 1411, 1711, 2557, 2680, 3443$, and 3528 keV, according to the new MSU ground-state mass of ^{56}Cu applied here. The associated uncertainty in the level energies was reduced to 12.3 keV (in this study 13 keV was adopted), which could be attributed to that adopted at 10 keV proton energy, E_p, and 7.1 keV S_p value. The energy levels in ^{56}Cu obtained experimentally and calculated by the shell-model are shown in Fig. 1. For comparison, the experimental data of the mirror nucleus ^{56}Co are also shown, and the mirror assignments are suggested accordingly.

Figure 1 shows an exceptional mirror symmetry of the excited states between ^{56}Cu and ^{56}Co. Therefore, the energies of the missing high-lying levels in ^{56}Cu can be assumed identical to the corresponding energies in the mirror ^{56}Co. Thus, for the missing levels in ^{56}Cu, we calculated their resonant rates using the level energies from ^{56}Co. To estimate the uncertainty in the level energies (E_X) of ^{56}Cu calculated by this approach, the neighboring mirror pairs in the *pf*-shell region [32] were analyzed. Figure 2 shows the level

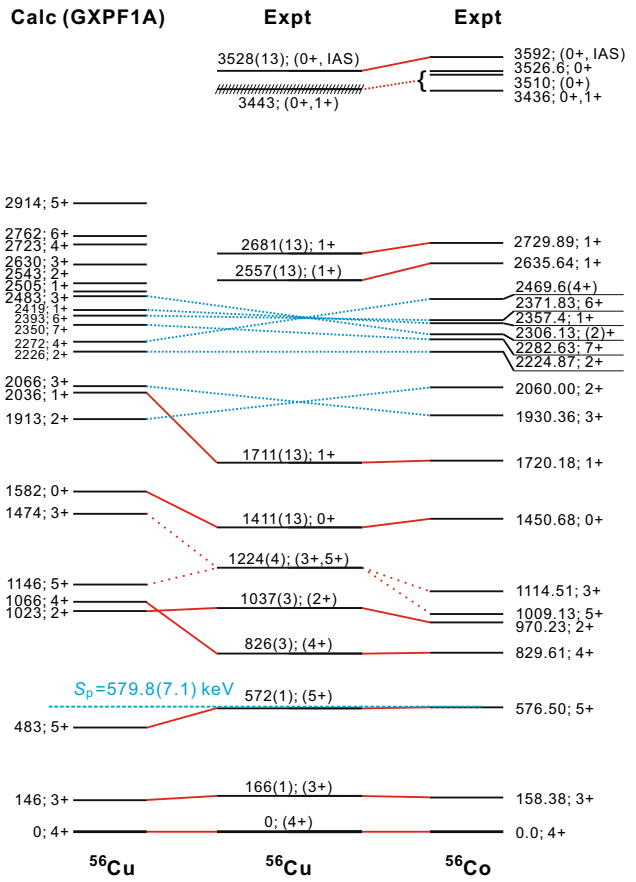

Fig. 1 (Color online) Energy levels in ^{56}Cu obtained experimentally and calculated by the shell-model. The experimental data are obtained from Ref. [30], as well as from Ref. [31] with corrections (shifted upward by 19.8 keV) discussed in the text; the exact results of the shell-model calculations with a GXPF1A interaction are obtained from Ref. [30]. The experimental data of the mirror nucleus ^{56}Co (obtained from NNDC website [32], see Ref. [33]) are shown for comparison, and the mirror assignment are suggested accordingly (the provisional values are indicated by dotted lines)

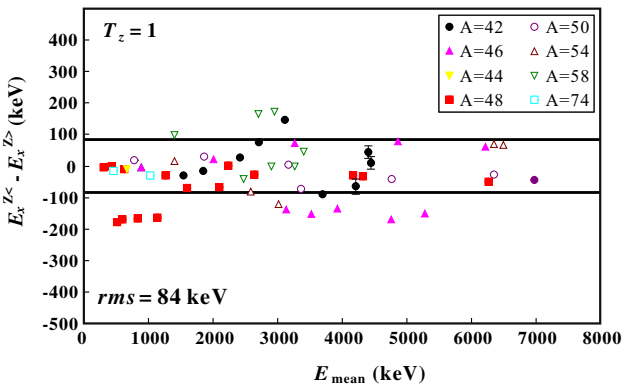

Fig. 2 (Color online) Level energy difference between mirror pairs of $T_z = 1$ for the *pf*-shell nuclei. The experimental level energies are obtained from the NNDC website [32]

energy difference between the mirror pairs of $T_z = 1$. The horizontal axis $E_{\rm mean}$ indicates the average level energies of the mirror pairs, and the vertical axis represents the level energy difference. The root-mean-square (*rms*) value was found to be ~ 84 keV. Thus, in this study, we assumed an uncertainty of ± 84 keV in the energies estimated for the missing states in ^{56}Cu, for which a provisional correspondence was demonstrated between the mirror ^{56}Co and shell-model calculated levels, shown in Fig. 1 by the dotted blue lines. In addition, we also adopted these shell-model level energies for six states of $E_{\rm X} > 2470$ keV (see Table 1) in the reaction rate calculations, and an *rms* uncertainty of 184 keV was estimated for these calculated levels, based on the energy difference between the experimental and shell-model levels in ^{65}Cu (the correspondence is shown in Table 1). However, their contribution to the total rate is negligible in the temperature region relevant to XRB, which is discussed in the next section.

5 Revised reaction rate

For a typical (p,γ) reaction, the total rate consists of the resonant and DC rates of proton capture on the ground state, and all thermally excited states in the target nucleus are weighted with their individual population factors [35, 40]. Here, the excitation energies in ^{55}Ni are rather high ($E_{\rm X} = 2089$ keV for the first excited state), and therefore the contributions from the thermally populated excited states can be entirely neglected in the temperature region relevant to XRB. The DC rate is also negligible compared to the resonant rate as demonstrated in previous works [24, 26]. Thus, only the resonant rate (equivalent to the total rate) was calculated in the temperature region relevant to XRB. In this work, we calculated the $^{55}\mathrm{Ni}(\mathrm{p},\gamma)^{56}\mathrm{Cu}$ resonant rate using the most accurate experimental value of $S_{\rm p}(^{56}\mathrm{Cu}) = 579.8 \pm 7.1$ keV [23], the recent experimental level energies in ^{56}Cu, the mirror information for the missing high-lying states in ^{56}Cu, and the previous shell-model results for six levels above $E_{\rm X} = 2470$ keV (see Table 1). A similar approach was used in Refs. [24, 34, 35].

The resonant $^{55}\mathrm{Ni}(\mathrm{p},\gamma)^{56}\mathrm{Cu}$ rate was calculated using Eq. (7) in Ref. [26], which is the well-known narrow resonance formalism given as [24, 34, 35]

$$N_{\rm A}\langle\sigma v\rangle_{\rm res} = 1.54\times10^{11}(\mu T_9)^{-3/2}\omega\gamma\exp\left(-\frac{11.605E_{\rm r}}{T_9}\right)\ [\mathrm{cm^3 s^{-1} mol^{-1}}], \quad (1)$$

where the unit of the resonant energy $E_{\rm r}$ and the strength $\omega\gamma$ is in MeV. The $E_{\rm r}$ value can be calculated by the relation of $E_{\rm r} = E_{\rm X} - S_{\rm p}$, where $E_{\rm X}$ denotes the level energies in ^{56}Cu (see Sect. 4), and the MSU value is $S_{\rm p}(^{56}\mathrm{Cu}) = 579.8 \pm 7.1$ keV. For the proton capture reaction, the reduced mass μ is defined by $A_{\rm T}/(1 + A_{\rm T})$ (here, the target mass is $A_{\rm T} = 55$ for ^{55}Ni). The resonant strength $\omega\gamma$ is defined as (Eq. (8) in Ref. [26])

$$\omega\gamma = \frac{2J+1}{2(2J_{\rm T}+1)}\frac{\Gamma_{\rm p}\times\Gamma_\gamma}{\Gamma_{\rm tot}}, \quad (2)$$

where $J_{\rm T}$ and J are the spins of the target ($J_{\rm T} = 7/2$ for the ground state of ^{55}Ni) and resonant state, respectively. The $\Gamma_{\rm p}$ and Γ_γ parameters are the partial widths for the entrance and exit channels, respectively, and $\Gamma_{\rm tot}$ is the total decay width of a resonance ($\Gamma_{\rm tot} \approx \Gamma_{\rm p} + \Gamma_\gamma$).

In this work, the gamma width Γ_γ for the part of the unbound state in ^{56}Cu was calculated by the available half-lives $T_{1/2}$ of the corresponding bound state in the mirror ^{56}Co using $\Gamma_\gamma = \ln 2 \times \hbar/T_{1/2}$, as shown in Table 1, where the previous shell-model gamma widths (Γ_γ) [30] are indicated in the parentheses of the corresponding Γ_γ column. It can be seen that the gamma widths calculated by the shell-model deviate from the mirror values by a factor of no more than ~ 3, except for a factor of 5.5 for the 1.411 MeV (0^+) state; however, this is not a noticeable parameter in the rate calculation, as discussed below. For the other remaining states listed in Table 1, the previous shell-model gamma widths (Γ_γ) [30] are adopted. In Ref. [30], the uncertainty for the calculated γ widths were estimated to be approximately a factor of two [37]. We conservatively estimated the uncertainty in the gamma widths adopted here as a factor of three; however, the uncertainties in the gamma widths obtained from the mirror half-lives $T_{1/2}$ are less than a factor of two.

The proton widths were calculated by the appropriate scaling to those in Ref. [30] enabled by the energy difference of $E_{\rm r}$ in the calculation of the penetrability factor P_ℓ. The leading uncertainties in $\Gamma_{\rm p}$ are due to those in $E_{\rm r}$ from the P_ℓ factors, and they are significantly larger than those resulting from the uncertainty due to the choice of channel radius r_0 and diffuseness a ($\sim 20\%$ [36]). In addition, the uncertainties in the C^2S factors calculated by the shell-model are estimated to be $\sim 20\%$ [37], which can be neglected in the present calculations. In Table 1, the corresponding uncertainties are indicated in the parentheses of the Γ_γ column. For example, the number 2.3 indicates an uncertainty factor of 2.3.

The resonant parameters for calculating the $^{55}\mathrm{Ni}(\mathrm{p},\gamma)^{56}\mathrm{Cu}$ reaction rate are listed in Table 1. The peak temperature in the recent hydrodynamic XRB models can be as high as ~ 1.4 GK [11, 38, 39]. In this study, we consider the reaction rate that is valid for a temperature

Table 1 Resonant parameters for calculating the ^{55}Ni(p, γ)^{56}Cu reaction rate

E_x(^{56}Cu, keV)	E_r (keV)[a]	J^π	$T_{1/2}$ (ps)[b]	Γ_γ (eV)[c]	$C^2S_p(\ell=1)$[d]	$C^2S_p(\ell=3)$[d]	Γ_p^e (eV)	$\omega\gamma$ (eV)
Experimental energy levels in ^{56}Cu obtained from Ong et al. [30]								$\omega\gamma \approx \omega\Gamma_p$
826(3)	246(7)	4^+	> 1.7	4.50×10^{-4}[f]	1.2×10^{-1}	6.9×10^{-1}	4.22×10^{-13}(2.3)	2.38×10^{-13}
1037(3)	457(7)	2^+	$0.12^{+0.12}_{-0.06}$	$3.80 \times 10^{-3}(0.1 \times 10^{-3})$	6.4×10^{-1}	1.6×10^{-1}	3.13×10^{-6}(1.4)	9.78×10^{-7}
1224(4)	644(8)	5^+	$0.38^{+0.14}_{-0.09}$	$1.20 \times 10^{-3}(2.0 \times 10^{-3})$		7.1×10^{-1}	2.40×10^{-5}(1.4)	1.62×10^{-5}
1224(4)	644(8)	3^+	$0.19^{+0.09}_{-0.06}$	$2.40 \times 10^{-3}(1.9 \times 10^{-3})$	1.5×10^{-1}		2.09×10^{-4}(1.3)	8.42×10^{-5}
Experimental energy levels in ^{56}Cu obtained from Orrigo et al. [31] with corrections								
1411(13)	831(15)	0^+	1580 ± 60	$2.89 \times 10^{-7}(16 \times 10^{-7})$		3.8×10^{-2}	2.28×10^{-5}(1.4)	1.78×10^{-8}
1711(13)	1131(15)	1^+	$0.34^{+0.35}_{-0.12}$	$1.34 \times 10^{-3}(0.5 \times 10^{-3})$		1.3×10^{-2}	5.64×10^{-4}(1.2)	7.44×10^{-5}
Estimated energy levels in ^{56}Cu by mirror symmetry as discussed in the text								$\omega\gamma \approx \omega\Gamma_\gamma$
1930(84)	1350(84)	3^+	$0.033^{+0.008}_{-0.007}$	$1.38 \times 10^{-2}(2.2 \times 10^{-2})$	5.9×10^{-1}	9.1×10^{-2}	2.58×10^{1}(2.1)	6.03×10^{-3}
2060(84)	1480(84)	2^+	0.024 ± 0.006	$1.90 \times 10^{-2}(1.4 \times 10^{-2})$	1.5×10^{-1}	5.7×10^{-1}	2.01×10^{1}(1.9)	5.93×10^{-3}
2225(84)	1645(84)	2^+		3.80×10^{-3}	1.7×10^{-3}	3.9×10^{-2}	7.64×10^{-1}(1.7)	1.18×10^{-3}
2283(84)	1703(84)	7^+		1.20×10^{-4}		9.9×10^{-3}	5.53×10^{-2}(1.8)	1.12×10^{-4}
2306(84)	1726(84)	3^+		8.90×10^{-3}	5.5×10^{-2}	1.3×10^{-2}	3.12×10^{1}(1.7)	3.89×10^{-3}
2357(84)	1777(84)	1^+		9.80×10^{-3}		1.0×10^{-2}	8.65×10^{-2}(1.8)	1.65×10^{-3}
2372(84)	1792(84)	6^+	0.042 ± 0.021	$1.09 \times 10^{-2}(3.1 \times 10^{-2})$		7.2×10^{-1}	6.92×10^{0}(1.7)	8.84×10^{-3}
2470(84)	1889(84)	4^+	0.016 ± 0.009	$2.85 \times 10^{-2}(5.3 \times 10^{-2})$	6.3×10^{-1}	1.3×10^{-1}	8.74×10^{2}(1.6)	1.60×10^{-2}
Levels in ^{56}Cu calculated by the shell-model obtained from Ong et al. [30]								$\omega\gamma \approx \omega\Gamma_\gamma$
2505(184[g])	1925(184)	1^+		2.00×10^{-2}		7.3×10^{-3}	1.52×10^{-1}(2.9)	3.31×10^{-3}
2543(184[g])	1963(184)	2^+		9.20×10^{-3}	1.6×10^{-2}	7.5×10^{-3}	3.06×10^{1}(2.5)	2.87×10^{-3}
2630(184[g])	2050(184)	3^+		9.60×10^{-3}	8.8×10^{-3}	3.6×10^{-3}	2.48×10^{1}(2.4)	4.20×10^{-3}
2723(184[g])	2143(184)	4^+		9.90×10^{-3}	2.3×10^{-2}	2.0×10^{-2}	9.55×10^{1}(2.2)	5.57×10^{-3}
2762(184[g])	2182(184)	6^+		1.50×10^{-2}		5.0×10^{-2}	3.40×10^{0}(2.4)	1.21×10^{-2}
2914(184[g])	2334(184)	5^+		1.70×10^{-2}	1.1×10^{-2}	1.0×10^{-2}	9.50×10^{1}(2.0)	1.17×10^{-2}

[a] Calculated by $E_r = E_x - S_p$ applying the MSU value of $S_p(^{56}\text{Cu}) = 579.8 \pm 7.1$ keV, the errors are indicated in the parentheses;

[b] Experimental $T_{1/2}$ values available for ^{56}Co;

[c] Calculated by $\Gamma_\gamma = \ln 2 \times \hbar / T_{1/2}$ using experimental $T_{1/2}$ values when they are available for ^{56}Co,
otherwise the shell-model results are adopted. For comparison, the nine values listed here in the parentheses are those calculated by the shell-model;

[d] Exact spectroscopic factors C^2S_p calculated by the shell-model obtained from Ref. [30];

[e] Appropriately scaled values to those calculated in Ref. [30] enabled by the energy difference in the penetrability factor P_ℓ, where the
leading uncertainties are estimated by considering those in E_r (from P_ℓ) and listed in the parentheses, e. g., number 2.3 indicates uncertainty of a factor of 2.3;

[f] Values obtained from previous shell-model calculations [30];

[g] The *rms* uncertainty of 184 keV is estimated for the levels calculated by the shell-model, based on the energy difference between the experimental and shell-model levels in ^{65}Cu

region up to 2 GK, corresponding to a Gamow peak of $E_r \approx 1.77$ MeV with a width of $\Delta \approx 1.28$ MeV [40]. Therefore, we believe that the resonances listed in Table 1 are sufficient for the description of the reaction rates of the relevant XRB region.

The percentage contributions of each resonance to the total resonant rate were calculated. Only five resonances contribute significantly to the total rate in the temperature region up to $\sim$2 GK: at $E_X = 826, 1037, 1224, 1930$, and 2060 keV. The contributions of these five special resonances to the total rate are shown in Fig. 3. Ong et al. provisionally assigned $E_x = 1224$ keV to either the $J^\pi = 3^+$ or the 5^+ state. The cases of 3^+ and 5^+ are shown in Figs 3(a) and 3(b), respectively. Only three resonances, at $E_X = 1037(2^+)$, $1224(3^+$ or $5^+)$, and $1930(3^+)$ keV dominate most of the temperature region relevant to XRB ($\sim$0.4–1.4 GK). If the $E_X = 1224$ keV state is of 3^+, it nearly dominates the entire temperature region relevant to XRB. If the $E_X = 1224$ keV state is of 5^+, the total rate can be reduced by a factor of $\sim$3 compared with the 3^+ case. Thus, the experimental determination of the J^π value is strongly required for the $E_X = 1224$ keV state. It should be noted that other resonances can also have noticeable contribution, which are not shown in Fig. 3, by considering the uncertainties in their E_r and $\omega\gamma$ values. A realistic reaction rate and the associated uncertainties were calculated and discussed in the following paragraph. It should be noted, that the rate by Ong et al. assumed the

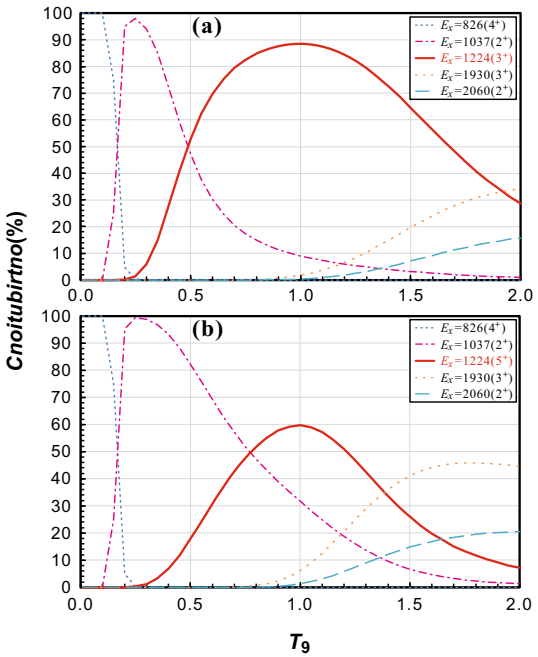

Fig. 3 (Color online) Percentage contribution of resonances to the total resonant rate. The five resonances (listed in Table 1) with significant contribution ($> 5\%$) are shown: **a** 3^+ for $E_X = 1224$ keV and **b** 5^+ for $E_X = 1224$ keV

$E_X = 1224$ keV state as a doublet (with 3^+ and 5^+), which might not be correct, according to the mirror information and shell-model calculations. This assumption probably results in an overestimation of the rate by different degrees depending on the assignment of this state to 3^+ or 5^+. Here, for comparison we also adopt the same assumption.

Table 2 summarizes the thermonuclear $^{55}\mathrm{Ni}(\mathrm{p},\gamma)^{56}\mathrm{Cu}$ rates calculated analytically using Eq. 1 with the resonant parameters listed in Table 1. The listed 1σ uncertainties (lower and upper limits) were calculated by a Monte Carlo method, which simultaneously sampled the uncertainties in E_r, Γ_p, and Γ_γ. Our (mean) rate can be parameterized very well by the standard format of [27]

$$\begin{aligned} N_A\langle\sigma v\rangle = \exp(&433.204 - 24.3787T_9^{-1} + 836.476T_9^{-1/3} \\ &- 1340.07T_9^{1/3} + 97.5459T_9 - 7.74309T_9^{5/3} \\ &+ 623.266\ln T_9) + \exp(4548.98 - 47.4577T_9^{-1} \\ &+ 3284.14T_9^{-1/3} - 8666.69T_9^{1/3} + 1011.96T_9 \\ &- 136.785T_9^{5/3} + 3156.30\ln T_9), \end{aligned} \quad (3)$$

with a fitting error less than 3.2% in the range of 0.1–2.0 GK.

Figure 4 shows a comparison of the rate in this study with two recently obtained results given in Refs. [23, 30]. It can be seen that our revised rate and associated uncertainties are rather different from those in the previous studies. The present uncertainties are significantly smaller than those by Ong et al. [30] mainly because we used a considerably more accurate experimental S_p value (and hence E_r) in the reaction rate calculations. Here, two remarks need to be made: (1) The recommended rate and uncertainties listed in Table IV in the paper by Ong et al. are not in exact agreement with those shown in Fig. 6 in the same paper, and the exact reason for this is not known and (2) according to the method of rate calculation described by Valverde et al. [23], we cannot reproduce the rate shown in Fig. 4 in their paper in any form. They used $S_p = 582.8(6.4)$ keV, which is only $\sim$3 keV higher than our value of $S_p = 579.8(7.1)$ keV. Our rate is expected not to be very different from that by Valverde et al. In the work by Valverde et al., if it is assumed that they used the exactly same Γ_p and Γ_γ parameters (instead of the scaled ones), we need to be able to approximately reproduce their rate within one or two factor. This suggests that Valverde et al. presented an incorrect rate and associated uncertainties in the figure. As there are no numerical rates listed in their tables, the exact reason for this is not known. Our rates are listed explicitly in Table 2.

Figure 5 shows a comparison of the rate in this study with five different rates available in the JINA Reaclib Database: *rath, thra, ths8, nifs, laur, ths8* rates. The uncertainties of the present rate are indicated by error bands in the figure. All rates

Table 2 Thermonuclear rates for the ^{55}Ni(p, γ)^{56}Cu reaction. The applied S_p values are listed in the parentheses

T_9	Present rate			JINA Reaclib rates				
	Mean (579.8 keV)	Lower limit	Upper limit	*nfis* (648 keV)	*rath* (−448 keV)	*thra* (1919 keV)	*laur* (459 keV)	*ths8* (648 keV)
0.10	4.59×10^{-19}	2.32×10^{-19}	1.42×10^{-18}	1.69×10^{-20}	7.07×10^{-27}	1.20×10^{-20}	3.37×10^{-21}	2.29×10^{-20}
0.15	4.56×10^{-15}	3.36×10^{-15}	1.00×10^{-14}	2.82×10^{-15}	1.04×10^{-18}	7.15×10^{-16}	3.06×10^{-15}	6.09×10^{-16}
0.20	5.42×10^{-12}	3.82×10^{-12}	8.80×10^{-12}	3.07×10^{-12}	8.58×10^{-15}	4.17×10^{-13}	3.15×10^{-12}	3.53×10^{-13}
0.30	2.09×10^{-08}	1.60×10^{-08}	2.96×10^{-08}	9.45×10^{-09}	8.73×10^{-11}	1.04×10^{-09}	1.34×10^{-08}	9.17×10^{-10}
0.40	1.52×10^{-06}	1.31×10^{-06}	1.97×10^{-06}	9.64×10^{-07}	1.33×10^{-08}	1.47×10^{-07}	1.77×10^{-06}	1.17×10^{-07}
0.50	2.49×10^{-05}	2.23×10^{-05}	3.07×10^{-05}	2.06×10^{-05}	3.66×10^{-07}	5.01×10^{-06}	3.69×10^{-05}	3.41×10^{-06}
0.60	1.79×10^{-04}	1.61×10^{-04}	2.16×10^{-04}	1.85×10^{-04}	4.03×10^{-06}	7.16×10^{-05}	2.85×10^{-04}	4.20×10^{-05}
0.70	7.50×10^{-04}	6.78×10^{-04}	9.01×10^{-04}	9.69×10^{-04}	2.53×10^{-05}	5.75×10^{-04}	1.22×10^{-03}	2.97×10^{-04}
0.80	2.21×10^{-03}	1.99×10^{-03}	2.65×10^{-03}	3.52×10^{-03}	1.08×10^{-04}	3.07×10^{-03}	3.62×10^{-03}	1.43×10^{-03}
0.90	5.08×10^{-03}	4.62×10^{-03}	6.12×10^{-03}	9.89×10^{-03}	3.53×10^{-04}	1.21×10^{-02}	8.36×10^{-03}	5.23×10^{-03}
1.00	9.86×10^{-03}	9.08×10^{-03}	1.20×10^{-02}	2.30×10^{-02}	9.39×10^{-04}	3.77×10^{-02}	1.63×10^{-02}	1.55×10^{-02}
1.10	1.70×10^{-02}	1.58×10^{-02}	2.09×10^{-02}	4.62×10^{-02}	2.14×10^{-03}	9.83×10^{-02}	2.82×10^{-02}	3.91×10^{-02}
1.20	2.71×10^{-02}	2.55×10^{-02}	3.40×10^{-02}	8.36×10^{-02}	4.31×10^{-03}	2.22×10^{-01}	4.49×10^{-02}	8.65×10^{-02}
1.30	4.10×10^{-02}	3.88×10^{-02}	5.26×10^{-02}	1.40×10^{-01}	7.88×10^{-03}	4.47×10^{-01}	6.72×10^{-02}	1.73×10^{-01}
1.40	5.97×10^{-02}	5.69×10^{-02}	7.96×10^{-02}	2.19×10^{-01}	1.33×10^{-02}	8.19×10^{-01}	9.63×10^{-02}	3.16×10^{-01}
1.50	8.48×10^{-02}	8.14×10^{-02}	1.18×10^{-01}	3.30×10^{-01}	2.11×10^{-02}	1.39	1.33×10^{-01}	5.40×10^{-01}
2.00	3.92×10^{-01}	3.87×10^{-01}	6.32×10^{-01}	1.68	1.10×10^{-01}	8.83	4.95×10^{-01}	3.71

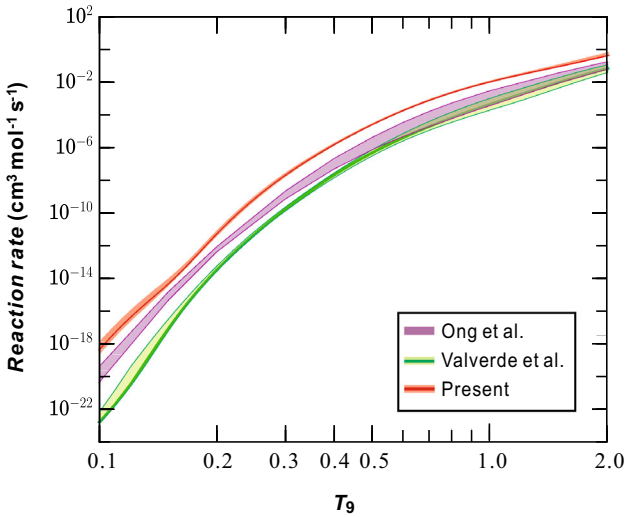

Fig. 4 (Color online) Comparison of the rate in this study and two recent results, Ong et al. [30] and Valverde et al. [23, 30]. The associated uncertainties are indicated by the colored bands. The rate in our study and the rate by Ong et al. (shown in Fig. 6 in their paper) are overlaid with that in Fig. 4 in the paper by Valverde et al. since the latter did not provide numerical rates

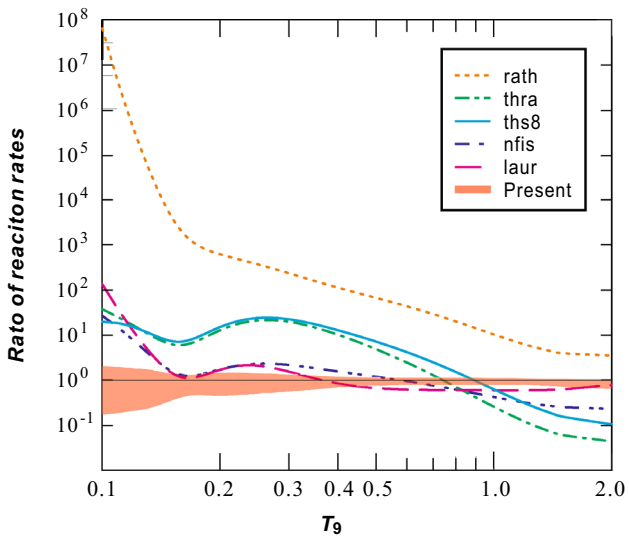

Fig. 5 (Color online) Ratios between the rate in this study and those compiled in the JINA Reaclib Database. The reference of unity is indicated by a solid black line. See text for details

for the ^{55}Ni(p, γ)^{56}Cu reaction are summarized in Table 2. It can be seen that neither the rates from the statistical model (*rath, thra, ths8*), nor that from the shell-model *nifs*, or the simple *laur* rate (based on the mirror information), agree with the rate in this study within the well-constrained uncertainties over the entire temperature region relevant to XRB. This implies that the experimental information of S_p, level structures, and ^{56}Cu properties are very important to determine the ^{55}Ni(p, γ)^{56}Cu rate more accurately.

6 Summary

The thermonuclear ^{55}Ni(p, γ)^{56}Cu rate was recalculated using the most accurate proton separation energy of $S_p(^{56}\mathrm{Cu}) = 579.8 \pm 7.1$ keV, the recent experimental levels in ^{56}Cu, together with the shell-model calculation and the mirror nuclear structure in ^{56}Co. Our revised rate deviates significantly from those available in the literature. To further reduce the uncertainties of the rate, the experimental determination of the J^{π} value (3^+ or 5^+) is strongly required for the crucial $E_X = 1224$ keV state in ^{56}Cu. In addition, we found that the previous reaction rate curve (Fig. 4 in Ref. [23]) is incorrect. Therefore, we recommend our revised rate to be incorporated in the future astrophysical network calculations, as it is based on a more fundamental experimental background. The astrophysical application of our revised rates in Type I XRB calculations is now under progress, which is beyond the scope of this work.

References

1. S.E. Woosley, R.E. Taam, Gamma-ray bursts from thermonuclear explosions on neutron stars. Nature **263**, 101 (1976). https://doi.org/10.1038/263101a0
2. P.C. Joss, X-ray bursts and neutron-star thermonuclear flashes. Nature **270**, 310 (1977). https://doi.org/10.1038/270310a0
3. H. Schatz, A. Aprahamian, V. Barnard et al., End point of the rp process on accreting neutron stars. Phys. Rev. Lett. **86**, 3471 (2001). https://doi.org/10.1103/PhysRevLett.86.3471
4. V.-V. Elomaa, G.K. Vorobjev, A. Kankainen et al., Quenching of the SnSbTe cycle in the rp process. Phys. Rev. Lett. **102**, 252501 (2009). https://doi.org/10.1103/PhysRevLett.102.252501
5. R.K. Wallace, S.E. Woosley, Explosive hydrogen burning. Astrophys. J. Suppl. **45**, 389 (1981). https://doi.org/10.1086/190717
6. H. Schatz, A. Aprahamian, J. Gorres et al., rp-process nucleosynthesis at extreme temperature and density conditions. Phys. Rep. **294**, 167 (1998). https://doi.org/10.1016/S0370-1573(97)00048-3
7. S.E. Woosley, A. Heger, A. Cumming et al., Models for type I X-ray bursts with improved nuclear physics. Astrophys. J. Suppl. **151**, 75 (2004). https://doi.org/10.1086/381533
8. W. Lewin, J. Paradijs, R.E. Taam, X-ray bursts. Space Sci. Rev. **62**, 223 (1993). https://doi.org/10.1007/BF00196124
9. T. Strohmayer, L. Bildsten, W. Lewin et al., *Compact Stellar X-Ray Sources* (Cambridge University Press, Cambridge, 2006)
10. A. Parikh, J. Jose, G. Sala et al., Nucleosynthesis in type I X-ray bursts. Prog. Part. Nucl. Phys. **69**, 225 (2013). https://doi.org/10.1016/j.ppnp.2012.11.002
11. A. Parikh, J. Jose, C. Iliadis et al., Impact of uncertainties in reaction Q values on nucleosynthesis in type I X-ray bursts. Phys. Rev. C **79**, 045802 (2009). https://doi.org/10.1103/PhysRevC.79.045802
12. H. Schatz, K.E. Rehm, X-ray binaries. Nucl. Phys. **A777**, 601 (2006). https://doi.org/10.1016/j.nuclphysa.2005.05.200
13. F. Pougheon, J.C. Jacmart, E. Quiniou et al., Direct observation of new proton rich nuclei in the region $23 \leq Z \leq 9$ using a 55 AMeV 58Ni beam. Z. Phys. A **327**, 17 (1987). https://doi.org/10.1007/BF01295244
14. B.A. Brown, R.R.C. Clement, H. Schatz et al., Proton drip-line calculations and the rp process. Phys. Rev. C **65**, 045802 (2002). https://doi.org/10.1103/PhysRevC.65.045802
15. J. Tian, N. Wang, C. Li et al., Improved Kelson–Garvey mass relations for proton-rich nuclei. Phys. Rev. C **87**, 014313 (2013). https://doi.org/10.1103/PhysRevC.87.014313
16. X.L. Tu, Y.A. Litvinov, K. Blaum et al., Indirect mass determination for the neutron-deficient nuclides ^{44}V, ^{48}Mn, ^{52}Co and ^{56}Cu. Nucl. Phys. A **945**, 89 (2016). https://doi.org/10.1016/j.nuclphysa.2015.09.016
17. A.H. Wapstra, G. Audi, The 1983 atomic mass evaluation: (I). Atomic mass table. Nucl. Phys. **A432**, 1 (1985). https://doi.org/10.1016/0375-9474(85)90283-0
18. G. Audi, A.H. Wapstra, The 1995 update to the atomic mass evaluation. Nucl. Phys. A **595**, 409 (1995). https://doi.org/10.1016/0375-9474(95)00445-9
19. G. Audi, A.H. Wapstra, C. Thibault, The AME2003 atomic mass evaluation (II). Tables, graphs and references. Nucl. Phys. A **729**, 337 (2003). https://doi.org/10.1016/j.nuclphysa.2003.11.003
20. M. Wang, G. Audi, A.H. Wapstra et al., The AME2012 atomic mass evaluation. Chin. Phys. C **36**, 1603 (2012). https://doi.org/10.1088/1674-1137/36/12/003
21. M. Wang, G. Audi, F.G. Kondev et al., The AME2016 atomic mass evaluation (II). Tables, graphs and references. Chin. Phys. C **41**, 030003 (2017). https://doi.org/10.1088/1674-1137/41/3/030003
22. Y.H. Zhang, P. Zhang, X.H. Zhou et al., Isochronous mass measurements of $T_z = -1$ fp-shell nuclei from projectile fragmentation of ^{58}Ni. Phys. Rev. C **98**, 014319 (2018). https://doi.org/10.1103/PhysRevC.98.014319
23. A.A. Valverde, M. Brodeur, G. Bollen et al., High-precision mass measurement of ^{56}Cu and the redirection of the rp-process flow. Phys. Rev. Lett. **120**, 032701 (2018). https://doi.org/10.1103/PhysRevLett.120.032701
24. L. Van Wormer, J. Gorres, C. Iliadis et al., Reaction rates and reaction sequences in the rp-process. Astrophys. J. **432**, 326 (1994). https://doi.org/10.1086/174572
25. R.H. Cyburt, A.M. Amthor, R. Ferguson et al., The JINA REACLIB database: its recent updates and impact on type-I X-ray bursts. Astrophys. J. Suppl. **189**, 240 (2010). https://doi.org/10.1088/0067-0049/189/1/240
26. J.L. Fisker, V. Barnard, J. Gorres et al., Shell model based reaction rates for rp-process nuclei in the mass range A = 44–63. At. Data Nucl. Data Tables **79**, 241 (2001). https://doi.org/10.1006/adnd.2001.0867
27. T. Rauscher, F.K. Thielemann, Astrophysical reaction rates from statistical model calculations. At. Data Nucl. Data Tables **75**, 1 (2000). https://doi.org/10.1006/adnd.2000.0834
28. P. Möller, J.R. Nix, W.D. Myers et al., Nuclear ground-state masses and deformations At. Data Nucl. Data Tables **59**, 185 (1995). https://doi.org/10.1006/adnd.1995.1002
29. J.M. Pearson, R.C. Nayak, S. Goriely et al., Nuclear mass formula with Bogolyubov-enhanced shell-quenching: application to r-process. Phys. Lett. B **387**, 455 (1996). https://doi.org/10.1016/0370-2693(96)01071-4
30. W.J. Ong, C. Langer, F. Montes et al., Low-lying level structure of ^{56}Cu and its implications for the rp process. Phys. Rev. C **95**, 055806 (2017). https://doi.org/10.1103/PhysRevC.95.055806
31. S.E.A. Orrigo, B. Rubio, Y. Fujita et al., Observation of the α-delayed γ-proton decay of ^{56}Zn and its impact on the Gamow–

Teller strength evaluation. Phys. Rev. Lett. **112**, 222501 (2014). https://doi.org/10.1103/PhysRevLett.112.222501
32. Evaluated Nuclear Structure Data File (ENSDF) Retrieval. http://www.nndc.bnl.gov/ensdf/
33. J. Huo, S. Huo, D. Yang, Nuclear data sheets for A = 56. Nucl. Data Sheets **112**, 1513 (2011). https://doi.org/10.1016/j.nds.2011.04.004
34. J.J. He, A. Parikh, B.A. Brown et al., Thermonuclear ^{42}Ti (p , γ)^{43}V rate in type-I X-ray bursts. Phys. Rev. C **89**, 035802 (2014). https://doi.org/10.1103/PhysRevC.89.035802
35. Y.H. Lam, J.J. He, A. Parikh et al., Reaction rates of ^{64}Ge (p , γ)^{65}As and ^{65}As (p , γ)^{66}Se and the extent of nucleosynthesis in type I X-ray bursts. Astrophys. J. **818**, 78 (2016). https://doi.org/10.3847/0004-637X/818/1/78
36. C. Iliadis, Proton single-particle reduced widths for unbound states. Nucl. Phys. A **618**, 166 (1997). https://doi.org/10.1016/S0375-9474(97)00065-1
37. C. Langer, F. Montes, A. Aprahamian et al., Determining the rp-process flow through ^{56}Ni : resonances in ^{57}Cu (p , γ)^{58}Zn identified with GRETINA. Phys. Rev. Lett. **113**, 032502 (2014). https://doi.org/10.1103/PhysRevLett.113.032502
38. A. Parikh, J. Jose, F. Moreno et al., The effects of variations in nuclear processes on type I X-ray burst nucleosynthesis. Astrophys. J. Suppl. **178**, 110 (2008). https://doi.org/10.1086/589879
39. J. José, F. Moreno, A. Parikh et al., Hydrodynamic models of type I X-ray bursts: metallicity effects. Astrophys. J. Suppl. **189**, 204 (2010). https://doi.org/10.1088/0067-0049/189/1/204
40. C.E. Rolfs, W.S. Rodney, *Cauldrons in the Cosmos* (University of Chicago Press, Chicago, 1988)